Imaging DNA Equilibrated onto Mica in Liquid using Biochemically Relevant Deposition Conditions

Patrick R. Heenan[†,‡] and Thomas T. Perkins[*,†,§]

[†]JILA, National Institute of Standards and Technology and University of Colorado, Boulder, Colorado 80309, United States

[‡]Department of Physics, University of Colorado, Boulder, Colorado 80309, United States

[§]Department of Molecular, Cellular, and Developmental Biology, University of Colorado, Boulder, Colorado 80309, United States

Abstract:

For over 25 years, imaging of DNA by atomic force microscopy (AFM) has been intensely pursued. Ideally, such images are then used to probe the physical properties of DNA and characterize protein-DNA interactions. The atomic flatness of mica makes it the preferred substrate for high signal-to-noise ratio (SNR) imaging, but the negative charge of mica and DNA hinders deposition. Traditional methods for imaging DNA and protein-DNA complexes in liquid have drawbacks: DNA conformations with an anomalous persistence length (p), low SNR, and/or ionic deposition conditions detrimental to preserving protein-DNA interactions. Here, we developed a process to bind DNA to mica in a buffer containing both $MgCl_2$ and KCl that resulted in high SNR images of equilibrated DNA in liquid. Achieving an equilibrated 2D configuration (*i.e.*, p = 50 nm) not only implied a minimally perturbative binding process, it also improved data quality and quantity because the DNA's configuration was more extended. In comparison to a purely $NiCl_2$-based protocol, we showed that an eight-fold larger fraction (90%) of 680-nm-long DNA molecules could be quantified. High-resolution images of select equilibrated molecules revealed the right-handed structure of DNA with a helical pitch of 3.5 nm. Deposition and imaging of DNA was achieved over a wide range of monovalent and divalent ionic conditions, including a buffer containing 50 mM KCl and 3 mM $MgCl_2$. Finally, we imaged two protein-DNA complexes using this protocol: a restriction enzyme bound to DNA and a small three-nucleosome array. We expect such deposition of protein-DNA complexes at biochemically relevant ionic conditions will facilitate biophysical insights derived from imaging diverse protein-DNA complexes.

KEYWORDS: atomic force microscopy, DNA, imaging, persistence length, protein-DNA complexes, and single molecule biophysics

Atomic force microscopy (AFM) is widely used to image and thereby characterize the properties of DNA and diverse proteins bound to DNA, including RNA polymerase, restriction enzymes, and nucleosomes.[1-16] Biophysical insights arise by acquiring images with a high signal-to-noise ratio (SNR) and rely upon preserving the native properties of protein–nucleic-acid complexes that can vary strongly with ionic conditions. Tapping-mode imaging in liquid rapidly emerged as the imaging modality of choice as it minimizes the lateral forces that can damage or disrupt fragile biological samples.[17] Unfortunately, a complementary and consensus method for preparing DNA and protein-DNA samples has yet to emerge. For instance, current protocols for imaging DNA in liquid capture DNA in compact, mechanically unequilibrated conformations that hinder analysis and interpretation. An ideal protocol would be rapid, preserve the native properties of the DNA and protein-DNA interaction in liquid, and yield high SNR images. Because of the lack of such an accessible protocol, protein-DNA complexes are still often imaged in air after rinsing them in ultrapure water,[18-20] a distinctly non-physiological protocol.

Mica is the preferred substrate for high SNR images due to the simplicity of generating clean, atomically flat substrates. For imaging in liquid, two main strategies have emerged to bind negatively charged DNA to negatively charged mica: mica derivatized with a positively charged silane[21] and Ni^{2+}-treated mica,[22,23] where Ni^{2+} ions have been preferred over Mg^{2+} due to stronger binding of the DNA to mica that facilitates imaging.[22] However, each technique presents important drawbacks. For instance, condensation and/or clumping of DNA can occur on silanized mica in the presence of divalent cations.[24] For Ni^{2+}-treated mica, it has been difficult to deposit and image DNA when monovalent cations are present.[25-27] Yet, numerous ensemble protein-DNA assays contain both $MgCl_2$ and a monovalent salt (*e.g.*, KCl or NaCl). Hence, to minimally perturb protein-DNA complexes, one should deposit them in a buffer containing both $MgCl_2$ and KCl and image in liquid, a difficult regime for AFM studies.

The benefits of silanized mica, including those prepared with silatranes,[28] are that they bind DNA under a relatively broad range of buffer conditions.[15,29] Two drawbacks of silanized mica are (*i*) the time needed to prepare silanized surfaces, and (*ii*) the reduced SNR of the images due to higher surface roughness, a drawback that is partially mitigated when using a more time-intensive

sample preparation process.[15,21,30] A notable recent application of silanized mica in liquid[15] was successfully deducing the correct persistence of DNA ($p \approx 50$ nm),[31] indicating such images can yield the native backbone stiffness of DNA. To do so, however, the authors needed to apply a 3D worm-like chain (WLC) model to analyze select 2D conformations of DNA. This analysis indicates the DNA was rapidly absorbed and thereby adopted a "kinetically trapped" polymer configuration.[9,15,29] If a 2D WLC model is used to analyze the fraction of interpretable conformations, then the derived p is ≈ 25 nm, well below the consensus value of p. As expected for such a low apparent p, kinetically trapped DNA molecules have a more compact configuration and thereby an increased number of multiple strand crossings that hinder analysis (Figure 1A, red). In contrast, if the deposition process achieves an "equilibrated" 2D WLC configuration, the conformations are more extended (Figure 1A, green) and thus a higher percentage of conformations that contain zero or one strand crossings. Quantitatively, a DNA molecule is defined as equilibrated if analysis of its 2D conformation with a 2D WLC model yields the correct of value of p, a definition consistent with prior DNA imaging studies.[15,32] Such equilibration is distinct from other studies that have observed real-time adsorption and desorption of local segments of DNA from bare mica in liquid.[33]

In Ni^{2+}-treated mica, the interstitial K^+ ions at the surface of the mica lattice are ion exchanged with Ni^{2+}, yielding a positively charged surface.[25,34] The DNA is typically deposited in the presence of ~1–20 mM $NiCl_2$.[22,34,35] The benefits of Ni^{2+}-treated mica are that it yields a higher SNR and requires less preparation time than silanized mica. There are, however, drawbacks:[15] (*i*) the resulting DNA configurations are kinetically trapped, when imaging in liquid;[32] (*ii*) non-physiological ionic conditions ($NiCl_2$ with little or no monovalent cations) are required to achieve sufficiently tightly bound DNA that in turn yields interpretable images;[15,22,25] and (*iii*) extensive tuning of buffer conditions.[22,25,36] For completeness, as noted above, a popular protocol deposits protein-DNA complexes onto Ni^{2+}-treated mica followed by rinsing with ultrapure water and then imaging in air.[35,37,38] While such a protocol has achieved equilibrated DNA when imaging in air,[32] we avoided this class of protocols to preserve native protein-DNA interactions. Moreover, a recent study shows partial conversion of DNA's structure from the traditional B-form to A-form when bound to Ni^{2+} treated mica in air.[24] Summarizing, the consensus in the field is that stable DNA

imaging on Ni^{2+}-treated mica requires a narrow window of ionic conditions (*e.g.*, Ni^{2+} cations in the absence of monovalent cations).[15,25,30]

Here, our goal was to develop a simple and reproducible protocol for acquiring high SNR images of equilibrated DNA in liquid when deposited at biochemically relevant ionic conditions (*e.g.*, 10 mM $MgCl_2$ + 25 mM KCl). Our protocol was not based on a single modification to an established deposition scheme, but instead on a set of changes including pre-incubating the mica with 100 mM $NiCl_2$, gentle rinsing, and never dewetting the sample. For increased robustness during imaging, we subsequently exchanged an equimolar concentration of $NiCl_2$ for $MgCl_2$. Analysis of the resulting DNA configurations yielded the correct persistence length (≈ 50 nm) when using a 2D WLC model and did so over a wide variety of monovalent salt concentrations. These equilibrated configurations were more extended (Figure 1B) than when 10 mM $NiCl_2$ replaced the 10 mM $MgCl_2$ in the deposition buffer (Figure 1C) or the DNA was deposited onto silanized mica (Figure 1D). Importantly, our protocol used only standard, commercially available reagents, took ~5 min, and worked over a range of DNA substrate lengths (300–2,000 bp) and in a standard commercial AFM. Unexpectedly, divalent cations in the imaging buffer were not required; we successfully imaged DNA on mica pre-incubated with 100 mM $NiCl_2$ when using an imaging buffer containing only monovalent ions albeit at some loss in data throughput and a reduction in p (35 nm). Biophysical applicability was demonstrated by imaging two protein-DNA complexes, a restriction enzyme bound to DNA and a small nucleosome array.

RESULTS AND DISCUSSION

We first present the final protocol, then discuss the process of achieving this protocol and how it generalizes to an unexpectedly broad range of ionic conditions for deposition and imaging, and finish by imaging a pair of protein-DNA complexes. In developing our protocol, we used two primary metrics: yield and persistence length. Yield was defined as the ratio of DNA configurations containing zero or one strand crossing divided by the number of total molecules fully contained within a set of images; such configurations facilitate analysis and the effect of proteins on the DNA conformation. Persistence length was determined from the 2D WLC model by analyzing the average tangent angle as a function of arc length along the DNA for molecules

displaying zero or one crossing (Figure S1).[32,39]Achieving a persistence length of ≈ 50 nm—in agreement with ensemble[31] and single-molecule force-spectroscopy[15,40,41] studies—would therefore reflect DNA bound to the mica in an equilibrated state (see Methods).

Rapid and biochemically relevant DNA deposition protocol. Our final protocol consisted of three main steps (Figure 2). In the first step, we placed a 20-µl drop of unbuffered 100 mM $NiCl_2$ onto freshly cleaved mica for 1 min followed by rinsing with ultrapure water and drying by touching the mica surface with filter paper. Importantly, this step— before depositing any DNA or protein-DNA complexes—was the only time the surface was dried and indeed the method of drying affected the final outcome (Figure S2). In the second step, we deposited a 20-µl drop of dilute DNA in Deposition Buffer [10 mM $MgCl_2$, 25 mM KCl, 10 mM HEPES (pH7.5)] onto the mica for 2 s before gently rinsing with 9 ml of Deposition Buffer (see Methods for details). Successful imaging of the DNA after such extensive rinsing demonstrated that DNA stayed attached to the Ni^{2+}-treated mica in the presence of 10 mM $MgCl_2$. Finally, in the third step, we rinsed the mica with Imaging Buffer [10 mM $NiCl_2$, 25 mM KCl, 10 mM HEPES (pH7.5)] where the $NiCl_2$-containing buffer trapped the equilibrated state of the DNA bound to the mica by increasing the DNA-mica interaction strength. This entire process starting from cleaving the mica to loading the sample into the AFM typically took ~5 min.

Improved protocol relies upon a series of refinements. Our final protocol evolved *via* a series of modifications that collectively were critical to achieving high yield while minimizing the influence of the substrate on the nanomechanics of the DNA, as evidenced by the deposited DNA adopting extended conformations with the correct persistence length. For conciseness, a subset of the deposition conditions tested are shown in Figure 3 to illustrate sequential improvement. Figure 3A shows representative images of the DNA configurations at select steps along this evolution accompanied by a summary of the deposition conditions at each step. The change in the conditions between the steps is highlighted in blue. Figures 3B and 3C report the yield and average persistence length of analyzed molecules. We note that these data (images, yield, and persistence length) were representative of our results at each step, not necessarily the best achieved. We did not optimize intermediate steps along the process but rather looked for a set of conditions that led to a simple

and robust deposition protocol at biochemically relevant conditions. In total, over 2,500 molecules were analyzed in this work when including the Supporting Information.

The starting point for our modifications featured ionic conditions typical of Ni^{2+}-treated mica protocol (10 mM $NiCl_2$ in the pre-treatment, deposition, and imaging buffers with a 2 mL rinse). As expected, these conditions resulted in a high proportion of kinetically trapped molecules that led to a low yield and persistence length (Figure 3A, Step 1). By increasing the concentration of $NiCl_2$ used to pre-treat the mica, we marginally increased the yield (Figure 3A, Step 2). Perhaps more importantly, we observed that the uniformity of the DNA on the surface dramatically increased (Figure S3), presumably because the higher $NiCl_2$ concentration overcame the previously described patchiness of Ni^{2+} on mica when incubating at 15 mM $NiCl_2$.[34] [Note, uniformly charged Ni^{2+}-treated mica may be broadly useful in a variety of AFM applications. As a proof of principle, we imaged the 2D lattice of bacteriorhodopsin (Figure S4)].

Next, we replaced the $NiCl_2$ in the deposition and imaging buffers with $MgCl_2$, which led to a fraction of the DNA molecules exhibiting the correct persistence length (Figure 3A, Step 3). However, the fraction of molecules exhibiting that equilibrated confirmation was low due, in part, to the weak DNA-mica interaction. In other words, these initial imaging experiments with only $MgCl_2$ in solution featured well-equilibrated DNA, but the DNA was too weakly bound for reliable tapping-mode imaging. We note that this intermediate finding is consistent with previous studies in air[32] and liquid,[22] though our final protocol does allow us to deposit and image in buffer containing $MgCl_2$ and KCl but, notably, no $NiCl_2$. In other words, $NiCl_2$ in the final buffer is not necessary but improves data quality by binding the DNA more strongly to the surface (Figure S5); successful imaging in $NiCl_2$ is therefore less stringent in its requirement of gentle imaging conditions (*e.g.*, low-amplitude tapping, see Methods for details).

We next combined the merits of depositing in $MgCl_2$ (to facilitate DNA equilibration) with imaging in $NiCl_2$ (for more robust imaging)(Figure 3A, Step 4). A useful analogy may be found in film photography, where an image is first developed before it is fixed or stabilized. In this analogy, the surface-bound DNA is the image, $MgCl_2$-based equilibration is the development process, and the $NiCl_2$-based imaging buffer is the fixing procedure. We continued to refine our

deposition process to enhance the yield of molecules showing only one or zero strand crossings by reducing the deposition time and increasing the DNA deposition concentration (Figure 3A, Step 5). Although the underlying mechanism for this improvement is unclear, it was experimentally reproducible across multiple samples on multiple days. Finally, we found that extensive (9 mL), but gentle, rinsing improved the equilibration of the DNA onto the mica (Figure 3A, Steps 6–7; see also Figure 2, Step 3). Introducing a small tilt during the extensive rinsing further improved yield, presumably because it helped avoid accidental dewetting (Figure S6) and the resulting high forces generated by a receding meniscus on a surface-bound DNA [*i.e.*, molecular combing (F > 65 pN)].[42,43]

High yield of equilibrated DNA on mica in liquid. By analyzing images acquired with our final protocol, we quantified the yield and the persistence length. The yield was 90% when imaging 680-nm-long DNA molecules [N = 142], an 8-fold improvement over depositing the DNA under identical DNA concentration and total ionic strength but substituting 10 mM $NiCl_2$ for the 10 mM $MgCl_2$ and rinsing with 2 mL of buffer (N = 116). Analysis of the DNA images yielded an average persistence length of 46.8 ± 0.6 nm (mean ± fitting error; N = 126)]. (Figure 3C; Figure S1), demonstrating the analyzed molecules had adopted a 2D equilibrated configuration on the mica. Indeed, of those molecules that contributed to the 90% yield, about 20% contained a looped configuration, consistent with expectations from a simple simulation that did not account for excluded volume effects (Figure S7). As a cross check, we deduced p from the distribution of end-to-end distances as a function of arc length, yielding p = 45 ± 4 nm [mean ± fitting error (Figure S8)] in quantitative agreement with p derived from the tangent vectors analysis. Finally, we note that the values for persistence and contour lengths obtained from human-annotation (see Supporting Information) were consistent with the values obtain using an automated analysis routine (Figure S9).[44]

High-precision measurements of DNA conformation. To quantify the SNR of the resulting images, we first measured the height of the DNA bound to mica using a metric based on the maximum height of each pixel along the spline defined along the full contour length of each molecule, rather than a single line or set of line scans per molecule (Figure S10A–B). The results

yielded 2.0 ± 0.3 nm [mean ± Std. Dev.; $N_{molecules}$ = 100 (Figure S10C)] in quantitative agreement with the DNA's width (2.0 nm).[45] Such agreement reflects the gentle imaging conditions, akin to earlier results that measured a height of 1.9 ± 0.2 nm when using peak-force tapping set to 40 pN,[27] with the advantage that the tapping-mode imaging used here leads to higher image acquisition rates. To quantify the noise, we measured the average surface roughness of bare mica, Ni^{2+}-treated mica, and ATPES-coated mica (Figure S11), yielding 1.14 ± 0.07 Å, 1.95 ± 0.06 Å and 4.3 ± 0.2 Å (mean ± Std. Dev.), respectively. Hence, we have measured the correct height for DNA and at a SNR of 10, a high SNR compared to traditional AFM imaging of DNA.[27]

To illustrate the quality of the resulting images, we show a gallery of representative DNA configurations (Figure 4A). The average persistence length for the six molecules shown is 50.8 ± 0.9 nm (mean ± SEM), similar to the persistence length determined for all molecules analyzed using the deposition protocol depicted in Figure 2. High-resolution scans of select segments of individual molecules revealed the right-handed helical structure of DNA (Figure 4B). The helical pitch of DNA has been previously resolved in liquid[27,46] with clearer images recently achieved when using frequency-modulated AFM.[47,48] Here, using tapping-mode imaging, we quantified the helical pitch of equilibrated DNA to be 3.51 ± 0.04 nm (mean ± SEM) (Figure S12) based on 15 images from 4 different molecules and 3 different cantilevers. Our result agrees with ensemble enzyme digestion studies that report a helical pitch of 3.6 nm.[49] This high-resolution study was facilitated by using a cantilever featuring a sharper tip radius [$r_{nom} \approx 2$ nm (Bruker SNL-10A)] than used in the rest of the paper [$r_{nom} \approx 8$ nm (Olympus BioLever Mini)] and by having the fast-scan axis parallel to the DNA axis. Approximately, one out of every three of these sharper cantilevers resolved the helical pitch of select DNA segments.

Quantification of the DNA's contour length agreed within 1% of the expected length (Figure S13), when using the standard rise per base pair for B-form DNA (0.34 nm/bp). [Note, as a counter example, DNA imaged in air on mica had a 20% reduction in contour length after depositing in $MgCl_2$ consistent with the DNA adopting a partial A-form structure, as confirmed by spectroscopic studies.][24] Successful application of our protocol was not restricted to relatively long DNA, but also worked well for 300-bp long DNA (Figure S14). Summarizing, we measured the correct

physical properties of DNA (persistence length, rise per base pair, width, and helical pitch) when imaging in liquid.

Depositing and imaging DNA under biochemically relevant ionic conditions. Our deposition protocol performed well across a wide range of monovalent and divalent combinations. For example, as the concentration of KCl in the deposition buffer was varied from 0 to 75 mM at fixed $MgCl_2$ concentration (10 mM), the yield and the persistence length remained essentially unchanged (Figure 5A–B), indicating the DNA continued to adopt an equilibrated conformation. A global fit to the dependence of p as a function of monovalent ionic strength[50] yielded 49.6 ± 0.4 nm (mean ± fitting error) (Figure S15), again consistent with an equilibrated 2D conformation. Equally important, the quality of the resulting images remained high (Figure 5C). At the highest KCl concentration tested (225 mM), the yield remained high but the persistence length decreased to ~35 nm (Figure 5A–B). At the higher KCl concentrations (≥ 75 mM), there were also some small surface artifacts (several nm wide by 1 nm tall), presumably salt crystals.

Unexpectedly, we could deposit and image in 3 mM $MgCl_2$ and 50 mM KCl (Figures S5), ionic conditions typical of many protein-DNA assays. As expected the persistence length remained approximately unchanged (~ 55 nm), but there was a reduction in yield to ~60% and successful imaging required gentle imaging conditions. We could also reduce or eliminate the divalent salt in the deposition and imaging buffers ($MgCl_2$ and $NiCl_2$, respectively) after pre-treating the mica with 100 mM $NiCl_2$. In the absence of any divalent cations, the yield was reduced from ~90% to ~50% and p decreased to ~35 nm, but the configuration of individual molecules remained well resolved (Figure S16). Overall, the robustness of our protocol to variations in KCl and divalent ion concentrations show that our methodology produced high-quality images of DNA deposited on Ni^{2+}-treated mica over a wide range of monovalent and divalent salt concentrations, a regime that was previously thought inaccessible. That said, it remains critical to deposit with $MgCl_2$ [or $CaCl_2$ (see below)] in lieu of $NiCl_2$ to equilibrate the DNA on the mica. Replacing $MgCl_2$ with $NiCl_2$ in our deposition buffer while keeping the rest of the final protocol the same led to kinetically trapped molecular configurations ($p \approx 25$ nm) (Figure S17), recapitulating earlier results.[32]

Imaging protein-DNA complexes in liquid. To demonstrate the broader applicability of our protocol, we next imaged two protein-DNA complexes: a restriction enzyme bound to DNA and a three-nucleosome array (Figure 6). Restriction enzymes, which cleave DNA at specific sequences, have been repeatedly studied by AFM.[8,11,51-53] BspMI is a type IIs restriction enzyme that binds to the sequence 5'-ACCTGC-3' and cleaves down stream of this recognition site. Cleavage occurs efficiently when BspMI binds to and bridges two recognition sites.[54] Like many restriction enzymes, BspMI can bind its recognition site without cleaving if Mg^{2+} is replaced by Ca^{2+}. Hence, to image BspMI bound to uncleaved DNA, we developed a 650-nm-long DNA with a single recognition site at its center and replaced $MgCl_2$ with $CaCl_2$ in our deposition buffer (see Methods for details). With these modifications, we acquired high-SNR images of BspMI bound to DNA in liquid (Figure 6A–B). As expected, BspMI bound to the center of individual DNA molecules. In addition, we observed DNA dimers formed by BspMI complexes bridging two separate DNA molecules (Figure 6C). This behavior is well established in ensemble studies.[54] More recently, AFM studies in air showed BspMI complexes bridging two separate binding sites after rinsing with ultrapure water.[18] Here, we can now visualize DNA bridging by BspMI imaged in liquid and do so with significantly higher SNR than the prior results in air. In addition, this result validates Ca^{2+} as an alternative divalent cation, as it also produced equilibrated DNA ($p \approx 52$ nm). Finally, building upon earlier AFM studies characterizing un-crosslinked nucleosomes in liquid,[55,56] we imaged nucleosomes bound to three high-affinity binding sites embedded in a 621-bp long DNA (Figure 6D).[57] Hence, the robustness and flexibility of our method permitted high-SNR imaging in liquid of a variety protein-nucleic acid complexes.

CONCLUSIONS

In summary, we deposited and imaged DNA in an equilibrated conformation on mica in liquid, implying a gentle deposition process. Equilibrated conformations were more extended and therefore easier to analyze when determining the DNA's configuration and the effect of proteins on that configuration. Importantly, we used a deposition buffer that contained both $MgCl_2$ and KCl, ionic conditions conducive to preserving native protein-DNA interactions. This success was not based on a single modification to an established protocol, but a set of changes including pre-

incubating the mica with 100 mM $NiCl_2$, drying with a filter paper, gentle rinsing, and never dewetting the sample. Imaging using such Ni^{2+}-treated mica yielded images with high SNR. To demonstrate the utility of this protocol, we imaged two protein-DNA complexes: a restriction enzyme bound to DNA and a nucleosome array. Looking forward, we speculate that the unexpectedly wide range of ionic conditions that yielded such images enables tuning the binding strength of the DNA to the surface, akin to earlier studies,[36] but in buffers containing both $MgCl_2$ and KCl. Such tuning, in turn, should facilitate studying the dynamics of protein-DNA complexes by AFM, in general, and by high-speed AFM, in particular,[36,58] at higher SNR coupled with conditions that preserve native protein-DNA interactions. Finally, our success in imaging protein-DNA complexes should immediately translate to the AFM studies of DNA origami and their applications.

METHODS

DNA samples. We purchased 300 and 2,000 base pairs (bp) DNA constructs that were HPLC purified (Fisher SM1621, SM1701). These DNAs were diluted to 50 ng/μL in TE Buffer [10 mM Tris-HCl (pH 8.0), 1 mM EDTA] and 20-μL aliquots were flash frozen and stored at -20 °C. Individual aliquots were thawed to room temperature and then stored at 4 °C for at most one week. For the BspMI assay, we developed a DNA construct from λ bacteriophage (NEB N3011S) by amplifying from position 9,887 to 11,785. This PCR-amplified 1,899 bp (≈ 650 nm) segment was chosen to position the BspMI recognition sequence (5'-ACCTGC-3') at the center of the resulting PCR product. After the DNA was purified *via* an agarose gel, the agarose was removed (Bio-Rad 7326165), the DNA was concentrated (Millipore UFC501024), and purified a final time (Qiaquick 28106) before elution into TE Buffer. The final DNA was diluted down to 180 nM in TE Buffer, aliquoted, and flash frozen.

DNA deposition protocol. We deposited the DNA as outlined in the text and illustrated in Figure 2. More specifically, we diluted the aliquoted DNA to 20 nM (for 2,000-bp DNA) or 80 nM (for 300-bp DNA) in our Base Buffer [10 mM HEPES (pH 7.5), 25 mM KCl] using KOH to adjust the pH. A higher concentration of smaller DNA was used to increase the number of molecules per image. We then cleaved 10-mm diameter mica (Ted Pella, 50) affixed to a metal puck (Ted Pella,

16218). We next placed a 20-µl drop of unbuffered 100 mM $NiCl_2$ (Sigma 654507) onto the freshly cleaved mica for 1 min followed by rinsing with 50 mL of ultra-pure water (18.2 MΩ, Barnstead GenPure Pro). The mica was then quickly dried by touching filter paper (Whatman 1002-042) to the center of the water droplet on the mica, and completely drying the surface. This step was the only time where the surface was allowed to partially or completely dewet. Immediately after drying, we deposited 20 µL of DNA in Deposition Buffer [10 mM HEPES (pH 7.5), 10 mM $MgCl_2$ + 25 mM KCl] where the concentration of the DNA was 1 nM for the 2,000-bp construct or 4 nM for the 300-bp construct. After 2 s, we gently rinsed the surface with ~1 mL of Deposition Buffer, tilted the surface to about 10°, and then gently rinsed with an additional 8 mL of Deposition Buffer. Care was taken during rinsing to avoid exposing any part of the surface to air or forces from a water droplet overcoming meniscus forces and/or rapidly flowing off of the side of the mica, which could perturb the sample and may cause salt to precipitate out of solution onto the surface. Finally, the surface was gently rinsed with 2 mL of Imaging Buffer [10 mM HEPES (pH 7.5), 10 mM $NiCl_2$ + 25 mM KCl]. Note, during deposition and rinsing, solutions were kept at room temperature (19 °C for the room containing our AFM). At all other times, the reagents were kept at 4 °C. Buffers were re-made each day from concentrated, 0.2-µm filtered stocks. For completeness, we note that we unexpectedly found that $NiCl_2$ solution made from seven-month-old $NiCl_2$ powder yielded poor results in comparison to a freshly purchased stock of $NiCl_2$ or a seven-month-old 1 M stock solution $NiCl_2$ (Figure S18).

The '$NiCl_2$ + KCl' protocol shown in Figure 1 and Figure 3 was prepared as above, except using a 10 mM $NiCl_2$ pre-treatment, and Imaging Buffer during deposition, rinsing, and imaging. Moreover, we only rinsed with 2 mL of Imaging Buffer, and omitted additional tilting and rinsing to better match more traditional $NiCl_2$ deposition conditions. The sample was dried using a filter paper as described above. To study DNA deposition on APTES-modified mica, we used our standard protocol, except substituting 0.1% APTES dissolved in water for 100 mM $NiCl_2$, and rinsing and imaging in the absence of divalent salt (*i.e.*, Base Buffer), as is typical with APTES-coated mica.[30] Before DNA deposition, the APTES-treated sample was also dried using a filter paper.

Depositing protein-DNA complexes. Importantly, we did not need to alter our deposition protocol for imaging protein-DNA complexes. The tri-nucleosome array was a gift of Anne Gooding and Tom Cech and based on published work from the Cech lab.[57] For depositing the tri-nucleosomes, we diluted them in Deposition Buffer to the same concentration used with the 300-bp DNA. The rest of the process, including deposition time, remained unchanged.

For the restriction-enzyme assay, we incubated 650-nm-long DNA at 20 nM with 40-fold diluted BspMI (New England BioLabs, R0502s, 50 units/mL incubation concentration) and 10 mM HEPES (pH 7.5), 10 mM $CaCl_2$ + 25 mM KCl as the buffer. After letting the enzyme and DNA incubate for 30 min at 30 ˚C, the deposition proceeded as described above, except with the $MgCl_2$ replaced by $CaCl_2$. Replacement of $MgCl_2$ with $CaCl_2$ allowed for site-specific binding but without cleavage (Figure 6A–C). When the same process was repeated in our standard Deposition Buffer, the DNA was cleaved due to the expected activity of BSP-MI in the presence of $MgCl_2$ (data not shown).

AFM imaging. We imaged all samples on a commercial AFM (Cypher ES, Asylum Research) featuring a temperature-controlled, closed-fluidic sample holder. Sample temperature was held at 19 °C. All images, except high-resolution images of the double helix, were obtained using an Olympus BioLever Mini (r_{nom} = 8 nm; k_{typ} = 90 pN/nm) with a 25-kHz resonance in liquid. For imaging the double helix, we used a Bruker SNL-10A ($r_{nom} \approx 2$ nm; k_{typ} = 350 pN/nm), which had a 16-kHz resonance in liquid.

Prior to imaging, we let the sample and cantilever settle for at least 30 min. All images were obtained in tapping mode with a typical set point amplitude of about 2 nm and a free amplitude of 150% of the set point. We chose the drive frequency as the closest peak of the drive transfer function to the thermal resonance when measured ~ 1 μm above the surface. All data presented in this paper used 2×2 μm^2 images with 512 pixels acquired at a 2-Hz scanning rate, except those of the double helix (Figures 4B & S12), images with protein-DNA complexes (Figure 6), and bacteriorhodopsin (Figure S4). The images of the double helix were taken with the same parameters, except the following changes: set point amplitude (~ 0.5–1 nm), free amplitude (~ 0.7–1.5 nm), and image size (20–100 nm). The images of bacteriorhodopsin or protein bound to

DNA used similar imaging parameters to the double helix, except the image size varied as follows: ~ 25 nm for bacteriorhodopsin, ~ 200 nm for the trinucleosomes, and ~ 600 nm for BspMI. The double helix images were taken with the fast-scan axis along the axis of the DNA to improve resolution by reducing low-frequency noise between line scans and tip-convolution artifacts.

Surface roughness of bare and treated mica. To quantify the difference in surface roughness between Ni^{2+}-treated mica and our APTES-coated mica, we created mica surfaces without adsorbed DNA and thereby measured the noise floor of our AFM measurement system in liquid as a function of surface treatment. The $NiCl_2$ and APTES test surfaces were prepared as described above, except omitting DNA in any of the buffers. As a control, we used unmodified mica that was rinsed and imaged in Base Buffer. All measurements that quantified the noise were obtained in the appropriate imaging buffers with the same individual cantilever on the same day. Other imaging parameters were consistent with the DNA experiments as discussed above, and we analyzed 3 images at each condition. As shown in Figure S11, bare mica showed the lowest surface roughness as measured by the standard deviation of the height [0.74 ± 0.03 Å (mean ± Std. Dev.)], with a measurable increase due to Ni^{2+}-treatment (1.18 ± 0.03 Å). As expected, the noise floor on APTES-coated mica was significantly higher (2.5 ± 0.1 Å).

Imaging bacteriorhodopsin. To see if Ni^{2+}-treated mica might be useful in other AFM applications, we imaged bacteriorhodopsin embedded in its native lipid bilayer, the prototypical protein for AFM studies of membrane proteins.[59] In initial experiments using standard bacteriorhodopsin imaging conditions (10 mM TrisHCl (pH 7.8), 150 mM KCl),[60] we resolved voids in the trimer lattice. Note, this proof-of-principle experiment was not optimized for image quality (Figure S4). Rather, we just wanted to demonstrate that the benefits of Ni^{2+}-treated mica were not limited to protein-DNA complexes.

Image analysis. We analyzed all AFM images of DNA using a semi-automated algorithm to determine the yield and persistence length. First, all DNA molecules fully contained within a single 2×2 μm^2 image were manually classified as either an interpretable individual DNA configuration that contained zero or one strand crossings (Figure 1, green), uninterpretable configurations that contained 2 or more strand crossings (Figure 1, red) or multiple overlapping individual DNA

molecules. We classified molecules with two or more loops as kinetically trapped due to their low apparent persistence length. Surface artifacts (*e.g.* a salt crystal) that could be reliably identified as not a DNA molecule were ignored. The yield, Y, was defined as:

$$Y = 100 * N_{\text{interpretable}}/(N_{\text{interpretable}} + N_{\text{uninterpretable}} + N_{\text{overlapping}}) \qquad \text{Eqn. 1}$$

where a yield of 0 indicates completely uninterpretable data, and a yield of 100 indicates completely interpretable data.

We quantified the angle θ between two tangent vectors separated by arc length s to measure the persistence length (p) of a molecule *via* AFM imaging (Figure 1A). The tangent vector was determined by fitting a third-order, least-squared polynomial spline through user-defined points spaced about every 10 nm along interpretable DNA molecules, excluding the looped sections of interpretable molecules that contained a loop (20%). The persistence length at a given condition was then obtained by a least-squares fit of the following equation for all interpretable molecules at that condition:

$$\ln(\langle\cos(\theta(s))\rangle) = -s/2p \qquad \text{Eqn. 2.}$$

The helical pitch was quantified by marking the position where the periodic structure of one DNA strand repeated. The position where a repeat crossed the axis of the DNA was manually bounded by two points, and the region in between these human-annotated points was fit with a parabola. The maximum of the parabola was considered the location of the repeat, where the fit was localized to a line of length 10 Å or less along the DNA axis. In other words, the human-annotated helical pitch location was refined by determining the local maximum in the DNA height from a parabolic fit. From two adjacent helical pitch locations on the same DNA strand, major pitch values were recorded as the total change in contour length. Both strands were measured separately in our estimation of the helical pitch.

Automated annotation. To verify that the human-annotated DNA contours were unbiased, we adapted a previously published method[44] for automated contour tracing. Briefly, the start and end of the each DNA were manually annotated. A second point near the start of the DNA molecule was needed to define an initial tangent. After determining an initial tangent vector, the algorithm

then iteratively update its estimation of the tangent vector until it reaches the opposite end of the DNA. The algorithm did not converge in roughly 20% of cases (*i.e.* took over 1000 steps of length 2 nm on a 680 nm piece of DNA), due to the presence of loops in DNA causing recursion. The analysis for the automatically generated contours was the same as described for the manually annotated data, except the computationally generated contour was used directly (*i.e.,* there was no spline interpolation for the automatically traced data).

ASSOCIATED CONTENT

Financial interest statement

The authors declare no competing financial interests.

Supporting Information

The Supporting Information is available free of charge on the ACS Publications website at DOI:

Eighteen supporting figures including the calculation of persistence length, the measured height of DNA, its contour length, and a multitude of different tested imaging conditions (PDF).

AUTHOR INFORMATION

Corresponding Author

*tperkins@jila.colorado.edu

ORCID

Patrick Heenan: 0000-0002-1720-0055

Thomas Perkins: 0000-0003-4826-9490

Author contributions

P.R.H. and T.T.P. designed the experiment. P.R.H optimized the assay conditions and acquired all of the data. P.R.H. developed the analysis techniques and algorithms. P.R.H. and T.T.P. wrote the manuscript.

ACKNOWLEDGMENTS

We thank Anne Gooding and Tom Cech for their gift of the trinucleosome array. This work was supported by the NSF (MCB-1716033, Phy-1734006) and NIST. Mention of commercial products is for information only; it does not imply NIST's recommendation or endorsement. T.T.P. is a staff member of NIST's Quantum Physics Division.

REFERENCES

(1) Hansma, H. G.; Vesenka, J.; Siegerist, C.; Kelderman, G.; Morrett, H.; Sinsheimer, R. L.; Elings, V.; Bustamante, C.; Hansma, P. K., Reproducible Imaging and Dissection of Plasmid DNA under Liquid with the Atomic Force Microscope. *Science* **1992,** *256*, 1180-1184.

(2) Hansma, H. G.; Bezanilla, M.; Zenhausern, F.; Adrian, M.; Sinsheimer, R. L., Atomic Force Microscopy of DNA in Aqueous Solutions. *Nucleic Acids Res.* **1993,** *21*, 505-512.

(3) Lyubchenko, Y. L.; Oden, P. I.; Lampner, D.; Lindsay, S. M.; Dunker, K. A., Atomic Force Microscopy of DNA and Bacteriophage in Air, Water and Propanol: The Role of Adhesion Forces. *Nucleic Acids Res.* **1993,** *21*, 1117-1123.

(4) Allen, M. J.; Dong, X. F.; O'Neill, T. E.; Yau, P.; Kowalczykowski, S. C.; Gatewood, J.; Balhorn, R.; Bradbury, E. M., Atomic Force Microscope Measurements of Nucleosome Cores Assembled Along Defined DNA Sequences. *Biochemistry* **1993,** *32*, 8390-8396.

(5) Guthold, M.; Bezanilla, M.; Erie, D. A.; Jenkins, B.; Hansma, H. G.; Bustamante, C., Following the Assembly of RNA Polymerase-DNA Complexes in Aqueous Solutions with the Scanning Force Microscope. *Proc. Natl. Acad. Sci. U.S.A.* **1994,** *91*, 12927-12931.

(6) Hansma, H. G.; Kim, K. J.; Laney, D. E.; Garcia, R. A.; Argaman, M.; Allen, M. J.; Parsons, S. M., Properties of Biomolecules Measured from Atomic Force Microscope Images: A Review. *J. Struct. Biol.* **1997,** *119*, 99-108.

(7) Kasas, S.; Thomson, N. H.; Smith, B. L.; Hansma, H. G.; Zhu, X.; Guthold, M.; Bustamante, C.; Kool, E. T.; Kashlev, M.; Hansma, P. K., Escherichia Coli RNA Polymerase Activity Observed Using Atomic Force Microscopy. *Biochemistry* **1997,** *36*, 461-468.

(8) Ellis, D. J.; Dryden, D. T.; Berge, T.; Edwardson, J. M.; Henderson, R. M., Direct Observation of DNA Translocation and Cleavage by the EcoKI Endonuclease Using Atomic Force Microscopy. *Nat. Struct. Biol.* **1999,** *6*, 15-17.

(9) Lysetska, M.; Knoll, A.; Boehringer, D.; Hey, T.; Krauss, G.; Krausch, G., UV Light-Damaged DNA and Its Interaction with Human Replication Protein A: An Atomic Force Microscopy Study. *Nucleic Acids Res.* **2002,** *30*, 2686-2691.

(10) Crampton, N.; Bonass, W. A.; Kirkham, J.; Rivetti, C.; Thomson, N. H., Collision Events between RNA Polymerases in Convergent Transcription Studied by Atomic Force Microscopy. *Nucleic Acids Res.* **2006,** *34*, 5416-5425.

(11) Sorel, I.; Pietrement, O.; Hamon, L.; Baconnais, S.; Cam, E. L.; Pastre, D., The EcoRI-DNA Complex as a Model for Investigating Protein-DNA Interactions by Atomic Force Microscopy. *Biochemistry* **2006,** *45*, 14675-14682.

(12) Miyagi, A.; Ando, T.; Lyubchenko, Y. L., Dynamics of Nucleosomes Assessed with Time-Lapse High-Speed Atomic Force Microscopy. *Biochemistry* **2011,** *50*, 7901-7908.

(13) Lyubchenko, Y. L., Preparation of DNA and Nucleoprotein Samples for AFM Imaging. *Micron* **2011,** *42*, 196-206.

(14) Ando, T.; Uchihashi, T.; Kodera, N., High-Speed AFM and Applications to Biomolecular Systems. *Annu. Rev. Biophys.* **2013,** *42*, 393-414.

(15) Murugesapillai, D.; Bouaziz, S.; Maher, L. J.; Israeloff, N. E.; Cameron, C. E.; Williams, M. C., Accurate Nanoscale Flexibility Measurement of DNA and DNA-Protein Complexes by Atomic Force Microscopy in Liquid. *Nanoscale* **2017,** *9*, 11327-11337.

(16) Shibata, M.; Nishimasu, H.; Kodera, N.; Hirano, S.; Ando, T.; Uchihashi, T.; Nureki, O., Real-Space and Real-Time Dynamics of CRISPR-Cas9 Visualized by High-Speed Atomic Force Microscopy. *Nat. Commun.* **2017,** *8*, 1430.

(17) Hansma, P. K.; Cleveland, J. P.; Radmacher, M.; Walters, D. A.; Hillner, P. E.; Bezanilla, M.; Fritz, M.; Vie, D.; Hansma, H. G.; Prater, C. B.; Massie, J.; Fukunaga, L.; Gurley, J.; Elings, V., Tapping Mode Atomic-Force Microscopy in Liquids. *Appl. Phys. Lett.* **1994,** *64*, 1738-1740.

(18) Wang, Y.; Ran, S.; Yang, G., Single Molecular Investigation of DNA Looping and Aggregation by Restriction Endonuclease BspMI. *Sci. Rep.* **2014,** *4*, 5897.

(19) Murugesapillai, D.; McCauley, M. J.; Huo, R.; Nelson Holte, M. H.; Stepanyants, A.; Maher, L. J., 3rd; Israeloff, N. E.; Williams, M. C., DNA Bridging and Looping by HMO1 Provides a Mechanism for Stabilizing Nucleosome-Free Chromatin. *Nucleic Acids Res.* **2014,** *42*, 8996-9004.

(20) Sukhanova, M. V.; Abrakhi, S.; Joshi, V.; Pastre, D.; Kutuzov, M. M.; Anarbaev, R. O.; Curmi, P. A.; Hamon, L.; Lavrik, O. I., Single Molecule Detection of PARP1 and PARP2 Interaction with DNA Strand Breaks and Their Poly(ADP-Ribosyl)Ation Using High-Resolution AFM Imaging. *Nucleic Acids Res.* **2016,** *44*, e60.

(21) Lyubchenko, Y.; Shlyakhtenko, L.; Harrington, R.; Oden, P.; Lindsay, S., Atomic Force Microscopy of Long DNA: Imaging in Air and under Water. *Proc. Natl. Acad. Sci. U.S.A.* **1993,** *90*, 2137-2140.

(22) Hansma, H. G.; Laney, D. E., DNA Binding to Mica Correlates with Cationic Radius: Assay by Atomic Force Microscopy. *Biophys. J.* **1996,** *70*, 1933-1939.

(23) Bezanilla, M.; Drake, B.; Nudler, E.; Kashlev, M.; Hansma, P. K.; Hansma, H. G., Motion and Enzymatic Degradation of DNA in the Atomic Force Microscope. *Biophys. J.* **1994,** *67*, 2454-2459.

(24) Japaridze, A.; Vobornik, D.; Lipiec, E.; Cerreta, A.; Szczerbinski, J.; Zenobi, R.; Dietler, G., Toward an Effective Control of DNA's Submolecular Conformation on a Surface. *Macromol.* **2016,** *49*, 643-652.

(25) Pastre, D.; Pietrement, O.; Fusil, S.; Landousy, F.; Jeusset, J.; David, M. O.; Hamon, L.; Le Cam, E.; Zozime, A., Adsorption of DNA to Mica Mediated by Divalent Counterions: A Theoretical and Experimental Study. *Biophys. J.* **2003,** *85*, 2507-2518.

(26) Pietrement, O.; Pastre, D.; Fusil, S.; Jeusset, J.; David, M. O.; Landousy, F.; Hamon, L.; Zozime, A.; Le Cam, E., Reversible Binding of DNA on $NiCl_2$-Treated Mica by Varying the Ionic Strength. *Langmuir* **2003,** *19*, 2536-2539.

(27) Pyne, A.; Thompson, R.; Leung, C.; Roy, D.; Hoogenboom, B. W., Single-Molecule Reconstruction of Oligonucleotide Secondary Structure by Atomic Force Microscopy. *Small* **2014,** *10*, 3257-3261.

(28) Shlyakhtenko, L. S.; Potaman, V. N.; Sinden, R. R.; Gall, A. A.; Lyubchenko, Y. L., Structure and Dynamics of Three-Way DNA Junctions: Atomic Force Microscopy Studies. *Nucleic Acids Res.* **2000,** *28*, 3472-3477.

(29) Lyubchenko, Y. L.; Shlyakhtenko, L. S., AFM for Analysis of Structure and Dynamics of DNA and Protein-DNA Complexes. *Methods* **2009,** *47*, 206-213.

(30) Lyubchenko, Y. L.; Shlyakhtenko, L. S.; Gall, A. A., Atomic Force Microscopy Imaging and Probing of DNA, Proteins, and Protein DNA Complexes: Silatrane Surface Chemistry. *Methods Mol. Biol.* **2009,** *543*, 337-351.

(31) Hagerman, P. J., Flexibility of DNA. *Annu. Rev. Biophys. Biophys. Chem.* **1988,** *17*, 265-286.

(32) Rivetti, C.; Guthold, M.; Bustamante, C., Scanning Force Microscopy of DNA Deposited onto Mica: Equilibration *Versus* Kinetic Trapping Studied by Statistical Polymer Chain Analysis. *J. Mol. Biol.* **1996,** *264*, 919-932.

(33) Vanderlinden, W.; De Feyter, S., Chain Relaxation Dynamics of DNA Adsorbing at a Solid-Liquid Interface. *Nanoscale* **2013,** *5*, 2264-2268.

(34) Billingsley, D. J.; Lee, A. J.; Johansson, N. A.; Walton, A.; Stanger, L.; Crampton, N.; Bonass, W. A.; Thomson, N. H., Patchiness of Ion-Exchanged Mica Revealed by DNA Binding Dynamics at Short Length Scales. *Nanotechnology* **2014,** *25*, 025704.

(35) Sushko, M. L.; Shluger, A. L.; Rivetti, C., Simple Model for DNA Adsorption onto a Mica Surface in 1:1 and 2:1 Electrolyte Solutions. *Langmuir* **2006,** *22*, 7678-7688.

(36) Lee, A. J.; Szymonik, M.; Hobbs, J. K.; Walti, C., Tuning the Translational Freedom of DNA for High Speed AFM. *Nano Res.* **2015,** *8*, 1811-1821.

(37) Cassina, V.; Seruggia, D.; Beretta, G. L.; Salerno, D.; Brogioli, D.; Manzini, S.; Zunino, F.; Mantegazza, F., Atomic Force Microscopy Study of DNA Conformation in the Presence of Drugs. *Eur. Biophys. J.* **2011,** *40*, 59-68.

(38) Christenson, H. K.; Thomson, N. H., The Nature of the Air-Cleaved Mica Surface. *Surf. Sci. Rep.* **2016,** *71*, 367-390.

(39) Landau, L. D.; Lifshitz, E. M., *Statistical Physics, 3rd Edition Part 1*. Pergamon Press: New York, 1980.

(40) Smith, S. B.; Finzi, L.; Bustamante, C., Direct Mechanical Measurements of the Elasticity of Single DNA Molecules by Using Magnetic Beads. *Science* **1992,** *258*, 1122-1126.

(41) Bustamante, C.; Marko, J. F.; Siggia, E. D.; Smith, S. B., Entropic Elasticity of λ-Phage DNA. *Science* **1994,** *265*, 1599-1600.

(42) Bensimon, A.; Simon, A.; Chiffaudel, A.; Croquette, V.; Heslot, F.; Bensimon, D., Alignment and Sensitive Detection of DNA by a Moving Interface. *Science* **1994,** *265*, 2096-2098.

(43) Bensimon, D.; Simon, A. J.; Croquette, V.; Bensimon, A., Stretching DNA with a Receding Meniscus: Experiments and Models. *Phys. Rev. Lett.* **1995,** *74*, 4754-4757.

(44) Wiggins, P. A.; van der Heijden, T.; Moreno-Herrero, F.; Spakowitz, A.; Phillips, R.; Widom, J.; Dekker, C.; Nelson, P. C., High Flexibility of DNA on Short Length Scales Probed by Atomic Force Microscopy. *Nat. Nanotechnol.* **2006,** *1*, 137-141.

(45) Sinden, R. R., *DNA Structure and Function*. Academic Press: San Diego, 1994.

(46) Mou, J.; Czajkowsky, D. M.; Zhang, Y.; Shao, Z., High-Resolution Atomic-Force Microscopy of DNA: The Pitch of the Double Helix. *FEBS Lett.* **1995,** *371*, 279-282.

(47) Ido, S.; Kimura, K.; Oyabu, N.; Kobayashi, K.; Tsukada, M.; Matsushige, K.; Yamada, H., Beyond the Helix Pitch: Direct Visualization of Native DNA in Aqueous Solution. *ACS Nano* **2013,** *7*, 1817-1822.

(48) Kuchuk, K.; Sivan, U., Hydration Structure of a Single DNA Molecule Revealed by Frequency-Modulation Atomic Force Microscopy. *Nano Lett.* **2018,** *18*, 2733-2737.

(49) Rhodes, D.; Klug, A., Helical Periodicity of DNA Determined by Enzyme Digestion. *Nature* **1980,** *286*, 573-578.

(50) Baumann, C. G.; Smith, S. B.; Bloomfield, V. A.; Bustamante, C., Ionic Effects on the Elasticity of Single DNA Molecules. *Proc. Natl. Acad. Sci. U.S.A.* **1997,** *94*, 6185-6190.

(51) Berge, T.; Ellis, D. J.; Dryden, D. T.; Edwardson, J. M.; Henderson, R. M., Translocation-Independent Dimerization of the EcoKI Endonuclease Visualized by Atomic Force Microscopy. *Biophys. J.* **2000,** *79*, 479-484.

(52) Crampton, N.; Yokokawa, M.; Dryden, D. T.; Edwardson, J. M.; Rao, D. N.; Takeyasu, K.; Yoshimura, S. H.; Henderson, R. M., Fast-Scan Atomic Force Microscopy Reveals That the Type III Restriction Enzyme EcoP15I is Capable of DNA Translocation and Looping. *Proc. Natl. Acad. Sci. U.S.A.* **2007,** *104*, 12755-12760.

(53) Neaves, K. J.; Cooper, L. P.; White, J. H.; Carnally, S. M.; Dryden, D. T.; Edwardson, J. M.; Henderson, R. M., Atomic Force Microscopy of the EcoKI Type I DNA Restriction Enzyme Bound to DNA Shows Enzyme Dimerization and DNA Looping. *Nucleic Acids Res.* **2009,** *37*, 2053-2063.

(54) Bath, A. J.; Milsom, S. E.; Gormley, N. A.; Halford, S. E., Many Type IIs Restriction Endonucleases Interact with Two Recognition Sites before Cleaving DNA. *J. Biol. Chem.* **2002,** *277*, 4024-4033.

(55) Kepert, J. F.; Toth, K. F.; Caudron, M.; Mucke, N.; Langowski, J.; Rippe, K., Conformation of Reconstituted Mononucleosomes and Effect of Linker Histone H1 Binding Studied by Scanning Force Microscopy. *Biophys. J.* **2003,** *85*, 4012-4022.

(56) Shlyakhtenko, L. S.; Lushnikov, A. Y.; Lyubchenko, Y. L., Dynamics of Nucleosomes Revealed by Time-Lapse Atomic Force Microscopy. *Biochemistry* **2009,** *48*, 7842-7848.

(57) Wang, X.; Paucek, R. D.; Gooding, A. R.; Brown, Z. Z.; Ge, E. J.; Muir, T. W.; Cech, T. R., Molecular Analysis of PRC2 Recruitment to DNA in Chromatin and Its Inhibition by RNA. *Nat. Struct. Mol. Biol.* **2017,** *24*, 1028-1038.

(58) Lyubchenko, Y. L.; Shlyakhtenko, L. S.; Ando, T., Imaging of Nucleic Acids with Atomic Force Microscopy. *Methods* **2011,** *54*, 274-283.

(59) Muller, D. J.; Engel, A., Atomic Force Microscopy and Spectroscopy of Native Membrane Proteins. *Nat. Protoc.* **2007,** *2*, 2191-2197.

(60) Muller, D. J.; Fotiadis, D.; Scheuring, S.; Muller, S. A.; Engel, A., Electrostatically Balanced Subnanometer Imaging of Biological Specimens by Atomic Force Microscope. *Biophys. J.* **1999,** *76*, 1101-1111.

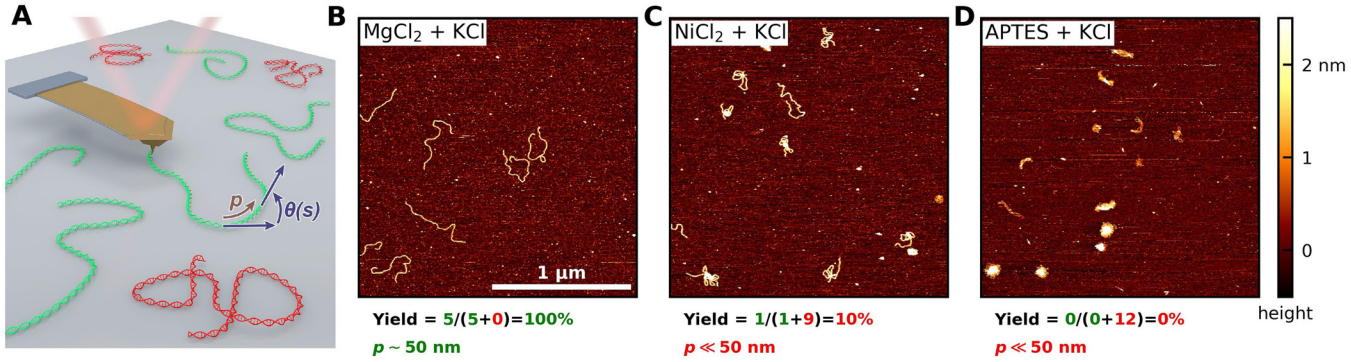

Figure 1. Configuration of DNA on mica depends on the details of the deposition process. (A) A cartoon illustrating AFM imaging of DNA in two different configurations: an extended, equilibrated one (green) and a compact, kinetically trapped one (red). Yield is defined as the ratio of DNA configurations containing one or zero strand crossings divided by the number of total molecules fully contained in a set of images. The persistence length (p), a measure of polymer backbone stiffness, is determined by the angle between tangent vectors (θ) along the path length s using a 2D WLC model. Credit: S. Burrows/JILA. (B) An AFM image of DNA in liquid when deposited under biophysically relevant ionic conditions (10 mM $MgCl_2$ + 25 mM KCl) and subsequently imaged in 10 mM $NiCl_2$ + 25 mM KCl after pre-treating the mica with 100 mM $NiCl_2$. The yield was high (90%) and analysis of the resulting DNA configurations yielded the correct persistence length (≈ 50 nm). (C) An image of DNA deposited on mica at 10 mM $NiCl_2$ + 25 mM KCl and imaged in the same buffer after gentle rinsing. (D) An image of DNA deposited at 25 mM KCl on mica coated with APTES. All solutions were buffered with 10 mM HEPES (pH 7.5). We note that these conditions were not optimized for the $NiCl_2$ deposition buffer and APTES-derivatized mica protocol used in panels, C–D respectively. All images are 2×2 μm^2 and are colored using the same vertical scaling. Acronym: APTES, (3-Aminopropyl)triethoxysilane.

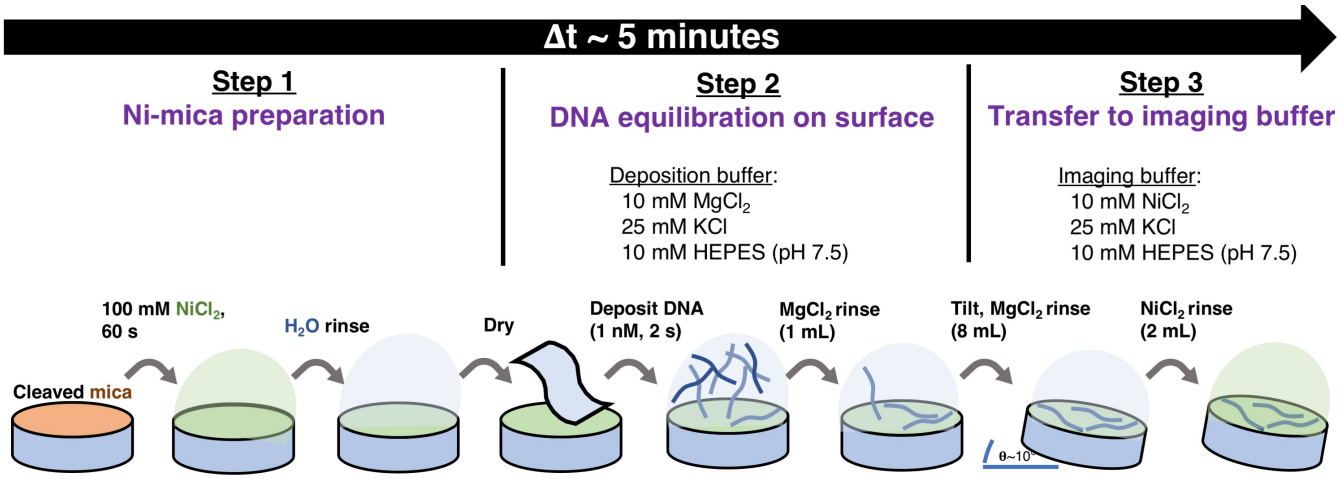

Figure 2. Rapid three-step protocol for preparing DNA for imaging on mica in liquid. This protocol consisted of three main steps. First, freshly cleaved mica was incubated with $NiCl_2$ at a ~10-fold higher concentration than traditionally used, rinsed with ultrapure water, and then gently dried. Second, dilute DNA was deposited onto the Ni^{2+}-treated mica at biochemically relevant ionic conditions and then the mica was extensively rinsed with deposition buffer. In the final step, the equilibrated configuration of the DNA was fixed for more robust imaging by increasing the interaction between the DNA and the mica by using an imaging buffer that contained 10 mM $NiCl_2$. As discussed in the text, imaging in $NiCl_2$ was not required.

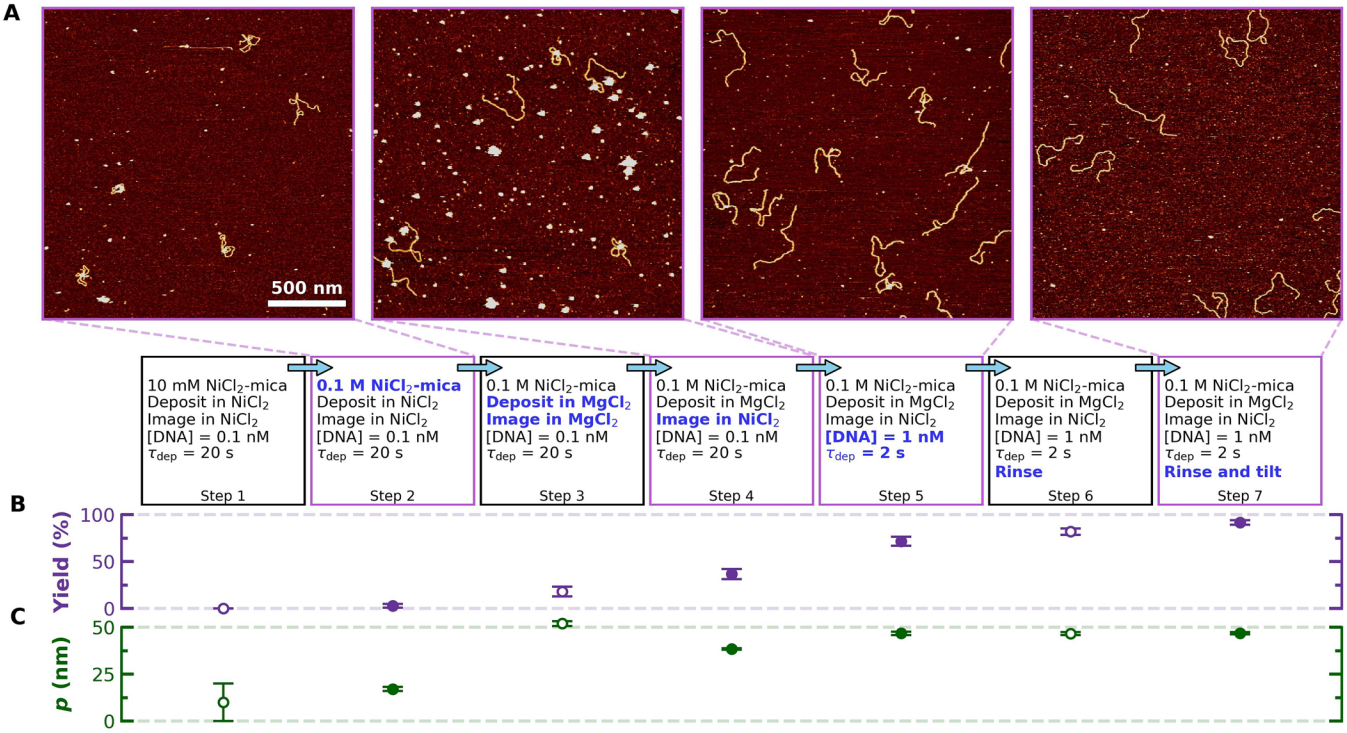

Figure 3. Improved DNA deposition required a sequence of refinements. (A) A set of tapping-mode images of DNA in liquid deposited under different deposition protocols as summarized in each box. The change between each deposition process is highlighted with blue text, and protocols associated with images are denoted with magenta boxes. (B–C) The percentage yield of interpretable DNA molecules and their corresponding persistence length (p) is depicted below each protocol. These values were computed from ~90 DNA molecules per condition with necessarily more images acquired at deposition protocols with a poor yield. Error bars represent the standard deviation for the yield and the fitting error for the persistence length. Persistence length was deduced using a 2D worm-like chain model. Solid symbols are associated with the images shown in panel A.

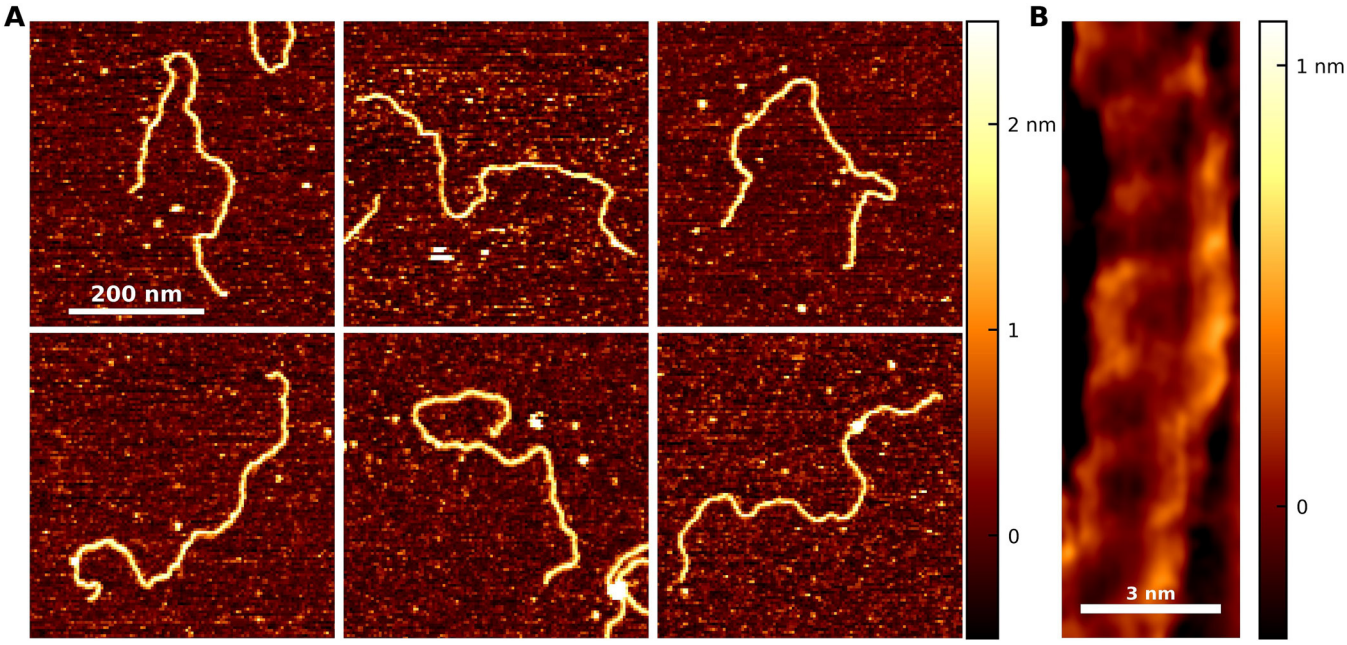

Figure 4. Images of individual DNA molecules highlight the resulting high signal-to-noise ratio. (A) A set of representative raw tapping-mode images of DNA in liquid selected from a larger scan area (2×2 μm^2) with traditional flattening. (B) An exemplary image of the double helix of DNA acquired using a tip featuring a sharper tip radius ($r_{nom} \approx 2$ nm) and smaller pixel size (0.5 Å) than those used in the remainder of the paper (see Methods). This image was fit with a third order, two-dimensional spline to subtract the background, then smoothed with a Gaussian with a width of two pixels (1 Å).

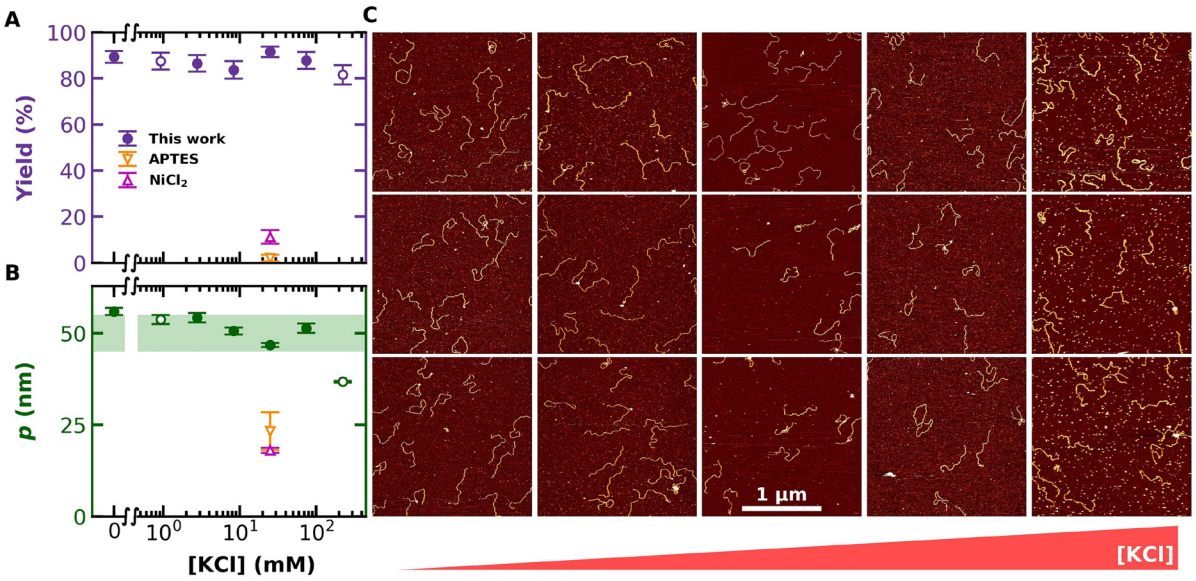

Figure 5. Equilibrated DNA deposited across a broad range of monovalent ionic conditions. (A–B) The percentage yield of interpretable DNA molecules and their corresponding persistence length (p) plotted as a function of monovalent ionic concentration at fixed $MgCl_2$ (10 mM). Closed symbols are associated with images shown in panel C. For comparison, yield and persistence length acquired under typical published conditions [10 mM $NiCl_2$ or APTES-functionalized mica] are shown. The $NiCl_2$ + KCl and APTES + KCl data points were determined from DNA deposited as in Figure 1C and 1D, respectively. Error bars represent the standard deviation. (C) Sets of three representative images plotted vertically acquired at 0, 2.8, 8.3, 25 and 75 mM KCl. Nanoscale precipitates became prevalent ≥75 mM KCl but the configuration of individual DNA molecules could still be traced and hence persistence length determined.

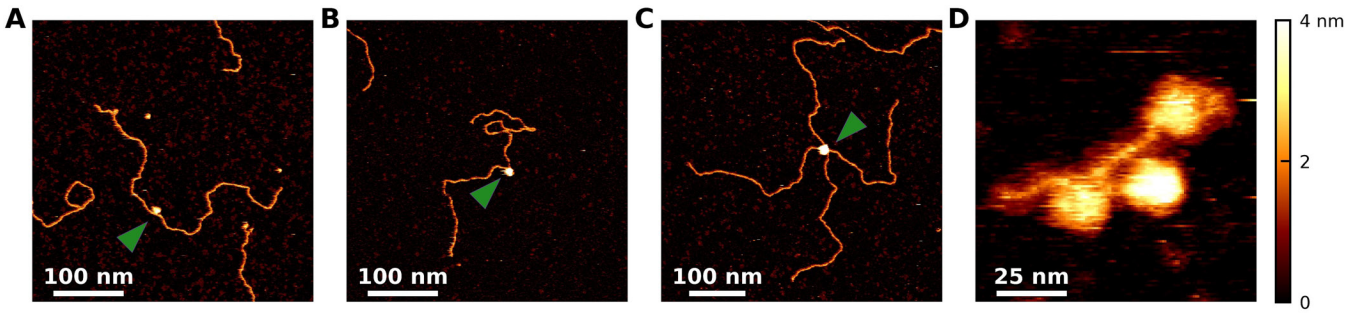

Figure 6. High signal-to-noise ratio images of protein-nucleic acid complexes deposited at biochemically relevant conditions. (A–B) Images of the type IIs restriction enzyme BspMI bound to a 650-nm-long DNA *via* the single recognition site located at the center of the DNA. $CaCl_2$ was substituted for $MgCl_2$ in the deposition buffer to suppress cleavage. (C) An image showing two separate DNA molecules bridged *via* a BspMI complex bound to two recognition sites. Such bridging is a key step to efficient cleavage by BspMI.[51] (D) An image of three nucleosomes on a 621-bp-long DNA substrate containing three high affinity binding sites for nucleosomes (*i.e.*, the 601 Widom sequence) deposited using our standard protocol containing $MgCl_2$ (Figure 2).

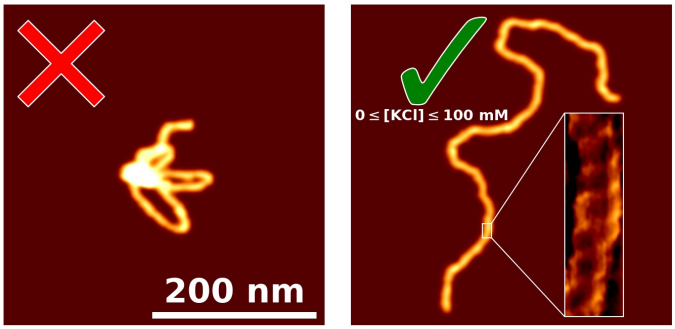

Table of contents graphic